Chronic VEGFR-3 signaling preserves dendritic arborization and sensitization under stress

Adri Chakraborty[1],[#], Raghavendra Upadhya[2],[#], Timaj A. Usman[1], Ashok K. Shetty[2], Joseph M. Rutkowski[1],[*]

[1]:Division of Lymphatic Biology, Department of Medical Physiology, Texas A&M University College of Medicine, Bryan, TX, USA

[2]:Institute for Regenerative Medicine, Department of Molecular and Cellular Medicine, Texas A&M University College of Medicine, College Station, TX, USA

Abstract

Dendritic arborization is critical for the establishment and maintenance of precise neural circuits. Vascular endothelial growth factor D (VEGF-D), well-characterized as a "lymphangiogenic" growth factor, reportedly maintains dendritic arborization and synaptic strength in the hippocampus of adult mice through VEGF receptor (VEGFR-3) signaling. Here, we investigated the effect of chronic VEGFR-3-specific activation on adipose arbor morphometry using the Adipo-VD mouse, a model of inducible, adipose-specific VEGF-D overexpression. We examined whether adipose tissue innervation was preserved or functionally different in Adipo-VD mice during stress in vivo and if VEGFR-3 signaling afforded neuroprotection to challenged neurons in vitro. Chronic VEGFR-3 signaling in Adipo-VD subcutaneous adipose tissue resulted in a reduction in the dendrite length, dendritic terminal branches (filament length), dendritic terminal branch volume (filament volume), but increased dendrite branching. We also identified reduced stimulus-evoked excitatory sympathetic nerve activity in Adipo-VD mice. Following 6-hydroxydopamine (6-OHDA) denervation, Adipo-VD dendritic arbors were preserved, including improved dendritic branch volume, length, and dendritic branches than in wildtype tissues. In vitro, we found that chronic elevation of VEGFR-3 signaling in developing mVC neurons changes the dendritic arbor complexity and improves stress-induced structure remodeling. Developing neurons are conferred neuroprotection against stress, potentially by upregulation of proteolytic conversion of pro-BDNF to mature BDNF. Mature neurons, however, display improved dendritic arbor complexity, and unaltered dendritic structural remodeling and improved resistance to stress with VEGFR-3 signaling. Overall, chronically increasing VEGFR-3 signaling in neurons has a synergistic impact on neurosensitization and neuroprotection during stress.

[*]Correspondence: Joseph M Rutkowski, Texas A&M University College of Medicine, 8447 Riverside Parkway, Bryan, TX 77807 USA, Ph: 979-436-0576, rutkowski@tamu.edu.
[#]denotes equal contribution

Keywords

VEGF-D; VEGF-C; neuroprotection; dendrite; arborization

INTRODUCTION

Neuropathy is a pathophysiological condition with increased incidence in aging, obesity, and diabetes-related disorders [1, 2]. One common thread in the etiology of peripheral neuropathy is chronic inflammation. Evidence shows inflammatory polyneuropathy causes maladaptive neuronal structural reorganization and central sensory circuit relays that may further propagate any pain phenotype [3, 4]. Locally hypersensitized sympathetic neurons remodel their arbor pattern and density in response to stress [5]. Structural remodeling of peripheral sensory neurons is therefore critical for afferent signaling output to the central nervous system [6].

Another common hallmark of chronic inflammatory disease is the induction of inflammation-associated lymphangiogenesis. Lymphatic vessels help to maintain tissue homeostasis through interstitial fluid balance and antigen and immune cell transport, making an expansion of the vessels likely to be beneficial during inflammation [7]. The primary lymphangiogenic pathway is through vascular endothelial growth factor receptor-3 (VEGFR-3) signaling by its ligands VEGF-C and -D. Blocking VEGFR-3 signaling in mice generally worsens and prolongs inflammation [8]. Due to its importance in lymphangiogenesis, VEGFR-3 signaling is often thought of as lymphatic-specific, but, interestingly, a host of studies have identified VEGFR-3 signaling to play multiple roles in neuronal growth and maintenance [9–11].

VEGFR-3 signaling has been identified in the brain and in neurons through various stages of growth. Expression of the VEGFR-3 ligand VEGF-C has been found in the developing brain [12, 13]. VEGF-C was shown to drive neurogenesis and activation in young neural stem cells [9, 12]. VEGF-D signaling through VEGFR-3 impacts dendritic arborization maintenance as demonstrated in both hippocampal-derived neurons in vitro and in the adult murine hippocampus in vivo [11]. Importantly, it was recently identified that VEGF-D is strongly downregulated following stroke and that pharmacologic VEGF-D delivery provides neuroprotection by preserving dendrite morphology and architecture [10]. With VEGFR-3 ligands upregulated in peripheral inflammation, might local dendritic arbor restructuring be an additional positive stress response to preserve tissue function beyond lymphangiogenesis?

To test whether VEGFR-3 signaling has the potential to act as a neuromodulator affecting innervation and neuroprotection, we made use of Adipo-VD mice (VEGF-D induction under an adipocyte-specific doxycycline-control transgene) under chow and high fed diet (HFD) conditions and human induced pluripotent stem cell - neural stem cell (hiPSC-NSC)-derived neurons in vitro. These systems permitted chronic VEGFR-3 activation to examine its effects on adipose innervation and dendritic arborization. Neurons were also challenged with 6-hydroxydopamine (6-OHDA), a dopaminergic and noradrenergic inhibitor that causes neurodegeneration, both in vivo and in vitro [14–16]. We identify that increased chronic

VEGFR-3 signaling improves dendritic arborization, branching, and crossings and affords neuroprotection and neurosensitization under inflammatory conditions.

MATERIALS AND METHODS

Animals and Diet

Mice with inducible, adipocyte-specific VEGF-D expression (Adipo-VD) have been previously described [17, 18]. Adipo-VD mice were used as hemizygous for the TRE-VEGF-D transgene and either wildtype or hemizygous for the *AdipoQ*-transgene as non-functional and functional mice and indicated as WT (−rtTA) and Adipo-VD (+rtTA), respectively, throughout the text and Figures. Age-matched male and female mice were used in each round of experiments and housed with 12-h light-dark cycles and ad libitum access to water and food in an AAALAC-approved facility. Starting at 6 weeks of age, all mice were fed a custom chow diet (Bio-Serv F4107; Bio-Serv, Flemington, NJ) or 60% kcal from fat diet [D16042102, lard based (supplemented D12492); Research Diets, Inc., New Brunswick, NJ], each containing 600 mg/kg doxycycline to control any off-target doxycycline effects. The diet was refreshed every 5-7 days to control for light-induced drug degradation. All studies were performed following 4 months of feeding (mice thus aged up to approximately 24 weeks) [18, 19]. Characterization of inflammatory and metabolic phenotype of these mice was performed in our previous studies [18, 19]. All animal study protocols were approved by the Institutional Animal Care and Use Committee at Texas A&M University (College Station, TX).

Pain Evoked Behavioral Test

To assess retraction nociceptive sensitization, a von Frey filament mechano-sensitization test [20, 21] was performed on the footpad of WT and Adipo-VD mice after 1 and 4 months of VEGF-D induction (n=10). The staff was trained locally by a laboratory with experience in the method [22]. Mechanical pressure thresholds (.007 to 300g) were measured using standardized von Frey filaments (Bioseb, Vitrolles, France) delivering increasing force when pushed onto the glabrous skin of the hind paw plantar surface at the same location for 1 second. Researchers were blinded to the genotype of the mice, but not to the diet or treatment conditions. Three trials were carried out per foot pad and the mechanical threshold sufficient to trigger paw retraction was noted. Changes in $\log_{10}$ threshold value were calculated and reported.

6-OHDA Nerve Ablation

6-OHDA is a dopaminergic and noradrenergic inhibitor that causes neurodegeneration and has been used centrally and, in the periphery, to acutely ablate neurons [15, 16]. Under isoflurane anesthesia, both dorsal inguinal adipose depots of chow fed mice were injected subdermally with 8 mg/ml (20 μl) 6-OHDA as instructed by a lab previously using the technique [16]. Mice were allowed to recover for 24 hours before von Frey filament mechano-sensitization testing.

Dorsal Root Ganglia Preparation and Imaging

Following perfusion with 4% PFA, lumbar (L3) dorsal root ganglia (DRG) were isolated from 4-month chow and high fat diet fed mice [23]. After 15% sucrose saturation, DRGs were embedded for cryosectioning. Sections (10 μm thick) were cut and mounted. L3 DRG were labeled with primary antibodies against Activating Transcription Factor (ATF3) (Table 1), with fluorophore-conjugated secondary detection and DAPI nuclear labeling. Immunofluorescence was imaged using an Eclipse E600 microscope (Nikon, Melville, NY) with images captured using cellSens Standard version 1.18 software (Olympus, Waltham, MS). Positive ATF3 nuclei labeling was identified by fluorescence thresholding kept the same across images in ImageJ. The percentage of ATF3 positive nuclei was manually counted in three random image fields for each condition. (n=4,4; 10 fields of view)

Adipose Tissue RNA and Protein Preparation

Following exsanguination, one subcutaneous, inguinal adipose tissue depot was harvested from 4-month doxycycline-fed mice. The inguinal lymph node was removed for an adipose-specific signature and the tissue was divided and flash-frozen immediately in liquid N_2. RNA and protein extraction was performed using adipose-specific methodology as previously [17].

Quantification of Norepinephrine Concentration

The concentration of norepinephrine was quantified by ELISA in the serum and inguinal adipose tissue homogenate according to the manufacturer's instructions (Rocky Mountain Diagnostics, USA). Tissue concentrations were normalized to the total sample protein (n=4-7).

Light Sheet Microscopy and Volume Analysis

Male whole inguinal adipose tissue depots were isolated. The lymph node was excised and the tissues were fixed in 4% paraformaldehyde for 24 hrs. and then transferred to 0.3% Triton X-100 in phosphate-buffered saline solution for 24 hrs. Female tissues were not used to avoid mammary duct associated neurons. Following incubation with a MAP-2 antibody (Table 1) for 48 hrs., the tissues were cleared using the PEGASOS tissue clearing method over 7 days [24] and imaged as a whole mount within the light sheet chamber. 3-D images were acquired under a 5x focal plane with normalized thresholding using a Zeiss Z.1 Light sheet microscope. The length and density of the dendrite and the cell bodies, respectively, were first determined using 10 visually isolated neurons in chow-fed tissue under 20x zoom under slice mode using the filament tracer tool in IMARIS software. These parameters were then applied throughout the analysis for all the other tissues irrespective of drug treatment. Whole tissue (n=3) image was semi-automatically traced for tissue neurons using automatic filament detection (an IMARIS plugin) and torch tool rendering autopath and autodepth. Based on the slice parameter inputs, the autopath tool automatically detected the dendrites and cell bodies determining the maximum diameter of the soma, and the start and end point diameter of the neurons. Visibly false processes along the edge of the tissues were manually deleted and removed from the calculations. The paths were auto-skeletonized and the images were 3-D reconstructed under maximum intensity projections to render the

final image product. Within each tissue, the combined number of individual neurons ranged from 200-860 across the volume. The neuron density of each tissue was normalized to the total tissue volume. The following measurements were assessed: dendrite length, dendrite branches, dendritic terminal branches (filament length), and filament volume (n=10).

hiPSC Neuronal Differentiation

The generation of neural stem cells (NSCs) from Human Induced Pluripotent Stem Cells (hiPSCs) was done as described previously [25]. hiPSC colonies (IMR90-4, Wisconsin International Stem Cell Bank) were grown on Matrigel coated plates as cell clumps using TeSR™-E8™ medium (StemCell Technologies, Canada) at a density of $2-2.5 \times 10^4$ cells/cm^2. There was no specific sex-based choice in selecting the hiPSC line utilized. Approximately 24 hours later, culture medium was changed to a neural induction medium containing neurobasal medium supplemented with 1x neural induction supplement (Thermo Fischer Scientific, USA) and changed every other day from day 0 to day 7. On day 7 of neural induction, primitive NSCs were dissociated with Accutase (Life Technologies) and plated on Matrigel-coated dishes in an NSC expansion medium as detailed in our recent study [26]. The NSC cultures were passaged every seven days, and the NSC characteristics at different passages was verified via immunofluorescence staining for nestin and Sox-2 [26]. Passage 7 (P7) NSCs were dissociated and plated on laminin-coated dishes at a density of 1×10^5 cells per cm^2 in an NSC expansion medium containing 50% neurobasal medium, 50% Advanced DMEM/F12, and 1x neural induction supplement and grown for 7 additional days (Thermo Fischer Scientific, USA). For developing hiPSC-NSC derived neurons, cells were cultured in normal neurobasal media containing 1X glutamax and 1X B27 with retinoic acid (Thermo Fischer Scientific, USA) for 31 days before use. While murine VEGF-D specifically signals VEGFR-3, human VEGF-D also activates VEGFR-2 [27]. Thus, the recombinant human VEGFR-3-specific mutant protein VEGF-C (Cys156Ser) (called "mVC" throughout the text) was used in vitro (R&D Systems;). PBS or mVC (1 µg/ml) was added to the media, with changes every 2 days until their maturation (Day 31). Maturation of the neurons were confirmed using MAP-2 labeling (Table 1). On day 31, the following treatments were set up in triplicates: a) untreated control b) 100 µM 6-OHDA for 30 mins c) chronic mVC control d) chronic mVC neurons +6-OHDA (30 mins). At day 31, the following treatments were set up in triplicates a) untreated control b) 100 µM 6-OHDA for 30 mins, to test the chronically cultured neurons, and c) 5 µg/ml mVC control (30 mins) d) mVC (5 µg/ml) + 6-OHDA (100 µM) for 30 mins, to test the impact of acute VEGFR-3 activation only. To study chronic VEGFR-3 activation on more mature hiPSC-NSC derived neurons, cells were first cultured for 31 days, followed by an additional 30 days with mVC (1 µg/ml) with media changes every 2 days. On day 62, the following treatments were set up in triplicates: a) untreated control b) 100 µM 6-OHDA for 30 mins c) chronic mVC control d) chronic mVC neurons +6-OHDA (30 mins).

Cell Viability Assay

Cell viability was assessed as per established protocol [28]. hiPSC-NSC derived neurons were seeded at 1×10^5 cells per cm^2 (a lower density) in 24 well plate for 31 days. Control and mVC neurons (+/− 6-OHDA) cells were treated with 0.5 µg/ml of propidium iodide for 5 minutes [29]. Counterstain, trypan blue (Life Technologies, Grand Island, NY, USA) was

applied for 5 sec as an exclusion assay. 3 random fields of view were captured using an Eclipse E600 microscope as described above. Dual stained cells were manually counted. No protein or RNA were extracted from this experiment.

Immunofluorescence of Neurons

hiPSC-NSC derived neurons were fixed with 5% paraformaldehyde for 15 minutes, blocked with 10% donkey serum, and immunolabeled with MAP-2, Tyrosine Hydroxylase, and PGP 9.5 antibodies (Table 1). Labeled neurons were visualized with fluorophore-conjugated secondary detection and imaged as above.

Morphometric Analysis

Dendritic arborization of in vitro neurons was measured by Sholl analysis on x10 and x40 magnification images of cultured neurons from 3 independent culture preparation using the Image J Sholl plugin for defined drug treatments (software version 1.52 -NIH, Bethesda, MD; *http://imagej.nih.gov/ij*). For each culture well 10 random fields were also captured at x10 and x40 magnification at the same exposure settings. The Simple Neurite Tracing function within NeuronJ (Image J plugin) [30] was used to trace the length of the dendrites from the soma. Individual images of single cell projections were skeletonized and the branch paths rendered using NeuronJ [30]. The Sholl mask starting points were rendered from the neuron soma with an overlap intersection gap of 20 μm. All of the analyses were performed by two blinded scientists with their results averaged. The following measurements were assessed using Sholl [31]: AUC, dendrite length (distance from soma), mean dendritic intersections and critical radius (the distance from soma at which the maximum number of dendritic intersections were measured) (n=10).

Quantitative Real-Time RT-PCR

Bio-Rad iTaq universal SYBR Green supermix (Bio-Rad Laboratories, Inc.) was used for adipose and hiPSC cDNAs in 5 μL reactions (Table 2) on a 384-well 7900T quantitative PCR machine (Applied Biosystems, Foster City, CA). Analyses of neurons and adipose tissues used *ACTB* and *Ubc*, respectively, as the most reproducible universal controls, with expression represented as 2-^{Ct} normalized to controls (n=5-8).

Protein Quantitation by Western Blot Analysis

Cellular protein homogenates were prepared in RIPA buffer and concentrations were determined by BCA Assay. Protein extracts from both tissues and cells were heated for 5 minutes at 95°C in Laemmli buffer containing β-mercaptoethanol. Total protein of 5 μg was loaded into wells of Mini-Protean TGX (Bio-Rad Laboratories, Inc.), or Novex Wedge Well 4% to 20% Tris-Glycine (Invitrogen, Carlsbad, CA) gels and separated by gel electrophoresis. Gels were transferred to nitrocellulose membranes (Bio-Rad), incubated with primary antibodies overnight (Table 1), labeled by the appropriate IR700 or IR800 Dye-conjugated secondary antibodies (LI-COR Biosciences, Lincoln, NE), and visualized on a LI-COR Odyssey scanner. Band densitometry was measured using Image Studio software version 4.0 (LI-COR Biosciences) and normalized to the β-actin signal for each sample. All sample values were then normalized to the controls within the experiment with

the exception of m-BDNF which is displayed as the raw densitometric value (as the controls yielded no value).

Statistical Analysis and Data Presentation

Study cohorts used 6-7 mice per group except as noted: 3 mice per group were used for Light sheet imaging due to tissue size, volume and IMARIS processing limitations; and cohorts of 4 mice per group were used for additional L3 DRG isolation. Genotyping was used to verify the AdipoQ-rtTA and TRE-VEGF-D transgene at termination, causing adjustments in the final planned group numbers. No differences were measured between male and female mice; only males were used in the imaging experiments. For in vivo direct comparison of cumulative distribution, unpaired t-test with Kolmogorov-Smirnov test was performed between the WT and Adipo-VD groups using GraphPad Prism software version 7.05 (GraphPad Software, La Jolla, CA). For in vitro direct comparisons, statistical significance was tested by an unpaired Welch's t-test, assuming unequal variance. For western blot data, densitometric analysis for drug treatments were normalized to controls set at value 1. For grouped in-vivo data, two-way ANOVA with multiple comparison of the means were performed with Sidak corrections. Statistical differences of the average areas under the curves were calculated for Sholl histograms with the Wilson/Brown correction. For grouped in vitro data, multiple comparison t-tests were performed with Holm-Sidak correction in Prism software. $P < 0.05$ was considered significant. Data are presented as means ± SD. Adipose neuron density data and raw neuronal characterization histograms from in vivo data display mean ± SE only for visual clarity.

RESULTS

Chronically elevated VEGF-D levels impact subcutaneous adipose tissue innervation

To investigate whether increased levels of VEGFR-3 ligand would impact adipose tissue innervation or neuronal phenotype, we utilized the Adipo-VD mouse model with chronic VEGF-D overexpression, about 4-fold over baseline [18], in adipose tissues for 4 months. Chow fed Adipo-VD (body weight: 26.6±0.4g) and WT (body weight: 25.4±0.9g) subcutaneous inguinal adipose tissues were extracted, the neurons immunolabeled, and the tissue volume 3-D imaged (Figure 1A). Dendrite tracing parameters were used to quantify changes in neuronal architecture (Figure 1A). Morphometric analyses identified a reduction in the dendrite length in Adipo-VD tissue (Figure 1B), with a significant increase in dendritic branches (Figure 1C). A nearly 3-fold reduction in dendritic terminal branches: filament length (Figure 1D) and filament volume (Figure 1E) were also measured. These analyses indicated dendritic arbor reorganization in the tissue with chronic VEGF-D signaling. RT-qPCR analysis identified increased transcriptional upregulation of *VEGFR-3,* a transcriptional downregulation of glutamatergic GluN2A and GluN2B genes (*Grin2a, Grin2b*), upregulation of the inhibitory GABA$_B$ receptor (*Gabbr1*), and a reduction of the GABA production enzyme *Gad2* in 4-month Adipo-VD adipose tissue compared to the WT (Figure 1F). No changes in the glutamatergic pathway-associated genes *Psd95* or *Ampa* and tyrosine kinase receptor gene *Ntrk2* were observed after 4 months of VEGFR-3 activation. To assess if there were any marked differences in sympathetic activity in response to the dendritic arborization changes tissue norepinephrine levels were measured. A significant

decrease in the norepinephrine level was observed in the AdipoVD inguinal adipose depot (Figure 1G). This effect appeared to be local to the tissue as circulating serum norepinephrine levels did not change (Figure 1H). Nuclear co-localization of the activating transcription factor 3 (ATF3) - a stand in for a functional readout of sympathetic neuropathy - was higher in Adipo-VD mouse L3 DRG compared to the WT and inversely correlated with norepinephrine levels (Figure 1I, J). Chronic VEGF-D overexpression in subcutaneous adipose tissue affects reorganization of neural structural innervation and dynamic dendritic rearrangements.

Neuronal differentiation in the presence of VEGFR-3 ligand results in minimal phenotypic change

To examine chronic VEGFR-3 signaling in vitro similar to what could be occurring in the Adipo-VD inguinal neurons, we used a model of neurons derived from Human Induced Pluripotent Stem Cells (hiPSCs) that had been cultured to neural stem cells (NSCs) [32]. Because human VEGF-D (and VEGF-C) have been shown to also interact with VEGFR-2 [27], we made use of the VEGFR-3-specific mutant VEGF-C (Cys156Ser) form (mVC) and differentiated hiPSC-NSCs in the presence of chronic VEGFR-3 ligand for 31 days. Differentiation to mature neurons was confirmed and appeared equivalent by PGP 9.5 and MAP-2 immunolabeling (Figure 2A). Previous work from other laboratories has identified a phenotypic shift toward dopaminergic neurons when cells were cultured in the presence of human full-length VEGF-C or VEGF-D [33, 34]. While we did observe some labeling of mVC-differentiated neurons for tyrosine hydroxylase, no obvious difference was identified in a dopaminergic neuronal shift when using the VEGFR-3-specific mVC (Figure 2A). This was confirmed genetically by RNA expression in which mVC-differentiated neurons had no difference in *TH* RNA expression, but rather an increase in *GAD1,* the gene encoding the 67kDa isoform of the GABA production enzyme, suggesting a GABAergic phenotype (Figure 2B). qPCR showed a reduction of *GluN2B* and an increase in *GluN2A* genes, suggesting a potential impact on long term potentiation associated signaling [35, 36]. Morphometric Sholl analysis demonstrated that mVC-differentiated neurons displayed longer, more complicated dendritic trees compared to the controls (Figure 2C). While the Sholl AUC measurement was significantly increased (Figure 2D), the average dendrite length (Figure 2E) and dendritic intersections Figure 2F) were unchanged among untreated and mVC groups. A trend toward an increased critical radius supported the other Sholl measurements indicating longer dendritic arbors for mVC neurons (Figure 2G). Developing neurons cultured in the presence of mVC, therefore, display increased arbor complexity and intersections upon long term VEGFR-3 activation.

Both developing and mature neurons cultured in the presence of chronic VEGFR-3 ligand display improved neuroprotection in vitro.

VEGFR-3 signaling was recently identified to afford potential neuroprotection following stroke [10]. To test if VEGFR-3 signaling confers a neuroprotective phenotype to neurons against stress, developing and mature neurons (+/− chronic mVC addition in the media) were challenged with the neurotoxic compound 6-hydroxydopamine (6-OHDA). For the developing neuron population, the viability of control neurons was visibly reduced compared to mVC-differentiated neurons (Figure 3A). Quantification of cell viability

confirmed that mVC neurons are more resistant to 6-OHDA treatment compared to the control neurons (Figure 3B). Control neurons that survived did not express tyrosine hydroxylase, indicating a loss of dopaminergic neurons (Figure 3C). Comparatively, surviving neurons cultured with mVC continued expression of tyrosine hydroxylase (Figure 3C), so dopaminergic neurons were comparatively protected from 6-OHDA stress. Surviving 6-OHDA-mVC neurons also expressed 2-fold higher levels of *VEGFR-3.* These neurons may have been those expressing *VEGFR-3* and afforded protection (and that those lost were not expressing it) as previously demonstrated that VEGFR-3 signaling was protective (Figure 3D)[10, 37]. Interestingly, these cells expressed significantly higher levels of brain-derived neurotrophic factor (BDNF) RNA (Figure 3E). BDNF, which plays an important role in dendritic dynamics and pruning, was also increased at the protein level in the presence of chronic VEGFR-3 ligand mVC. (Figure 3F) [38–40]. While the pro-BDNF levels were consistent across all the treatment groups (Figure 3F, G), mVC-differentiated neurons expressed significantly more mature-BDNF (m-BDNF) compared to the controls (Figure 3F, H). The relative expression of m-BDNF was higher in mVC neurons compared to the controls irrespective of 6-OHDA treatment (Figure 3H). Morphometric analysis using Sholl analysis demonstrated that 6-OHDA-mVC neurons display a simplified dendritic arbor complexity, dendrite arbor shrinkage and a reduced length compared to the 6-OHDA control (Figure 3I). Sholl AUC measurement (Figure 3J) and dendrite length (Figure 3K) were significantly reduced. No changes in the average number of dendritic intersections and the critical radius were measured (Figure 3I, 3L). Developing mVC neurons, therefore, by changing the dendritic arbor complexity, display improved stress-induced structure remodeling through VEGFR-3 signaling.

Mature neurons cultured for 30 days with mVC displayed unchanged morphometry upon 6-OHDA treatment suggesting improved neuroprotection (Supplementary Figure 1 A, B). Sholl analysis demonstrated that mature mVC dendritic arbor complexity did not change upon 6-OHDA treatment (Supplementary Figure 1 A). Sholl AUC measurements, dendrite length (Supplementary Figure 1 C), intersections (Supplementary Figure 1 D) and critical radius. (Supplementary Figure 1 E) also remained unchanged by stress. Mature mVC neurons, therefore, displayed improved dendritic arbor complexity, and unaltered stress-induced structure remodeling, with long term VEGFR-3 activation.

Acute VEGFR-3 signaling does not demonstrate neuroprotection

To test if an acute VEGFR-3 signal could elicit a similar neuroprotective effect, day 31 mature neurons cultured in the absence of additional VEGFR-3 ligands were treated with mVC for 30 minutes followed by a 30 minute 6-OHDA challenge. Surprisingly, acute mVC treatment was able to elicit some morphometric changes within 60 minutes akin to chronically mVC-cultured neurons that were confirmed by Sholl analysis (Figure 4A, B). Upon 6-OHDA neurotoxicity, however, acute VEGFR-3 activation failed to elicit morphometric neuroprotection against stress (Figure 4B). Caspase-3 protein cleavage, indicative of apoptosis initiation, were significantly elevated with 6-OHDA regardless of mVC addition (Figure 4C, D). The Sholl AUC (Figure 4E) and dendrite length (Figure 4F) demonstrated an acute mVC effect, with 6-OHDA challenged neurons displaying a significant reduction in branch complexities and shorter dendrites regardless of VEGFR-3

ligand. Dendritic intersections were also reduced (Figure 4G) indicating pruning or dendritic structure destabilization during stress. Dendrite critical radius also remained unchanged across control and mVC neurons irrespective of treatment (Figure 4H).

Protein immunoblotting data (Figure 4I) demonstrated that acute mVC treatment had no effect on the expression of total VEGFR-3 (Figure 4J) with a small amount of Akt (Figure 4K) and ERK phosphorylation (Figure 4L) detectable 60 minutes post-treatment. 6-OHDA treatment induced stress significantly reduced the expression of VEGFR-3, GluN2B, and pro-BDNF expression in control and mVC treated neurons (Figure 4J, M, N). The expression of VEGFR-3, GluN2B, and pro-BDNF protein was significantly higher in mVC neurons compared to the 6-OHDA group similar to neurons differentiated with chronic VEGFR-3 ligand. No quantifiable m-BDNF was detected with acute mVC. Under these experimental conditions, only minimal VEGFR-3 receptor-mediated neuroprotective effects were seen with acute VEGFR-3 activation in mature neurons.

Chronic VEGF-D overexpression protects inguinal adipose innervation against acute injury.

Despite acute treatment not affording significant protection, the neuroprotective phenotype demonstrated by chronic VEGFR-3 signaling in cultured neurons led us to test neuroprotection in Adipo-VD mice in which VEGF-D had been overexpressed for 4-months. Chow fed WT and Adipo-VD subcutaneous adipose depots were denervated with a single 6-OHDA injection in a separate cohort of mice as previously demonstrated [15, 16, 41]. The tissue was volume imaged for MAP-2 sympathetic innervation and dendrite density appeared to be maintained (Figure 5A). Quantitative morphometric analysis between untreated control and 6-OHDA tissue identified a significant increase in dendritic length and reduced dendritic branching, dendritic terminal filament length, and total dendritic terminal volume (Supplementary Figure 2 A, B, C, D). The same analysis comparing WT and Adipo-VD mice following 6-OHDA tissue injections identified significantly shorter dendrite arbor length in Adipo-VD tissue (Figure 5B). A significantly higher dendrite branch number (Figure 5C), dendrite terminal filament length (Figure 5D), and total dendrite terminal filament volume (Figure 5E) were observed in Adipo-VD mice.

Since activity-mediated restructuring of the dendritic tree influences synaptic connectivity and signals integral to sympathetic outflow, norepinephrine levels were measured as a functional readout of sympathetic function. Norepinephrine levels were 3-fold higher in the Adipo-VD subcutaneous adipose tissue than WT mice following 6-OHDA stress (Figure 5F). Serum levels of NE were also marginally higher (Figure 5G). ATF3 nuclear co-localization in the L3 dorsal root ganglia, as a functional readout for sympathetic neuropathy, was 8-fold lower in 6-OHDA injected Adipo-VD mice than WT (Figure 5H, 5I). Increased sympathetic sensitivity in Adipo-VD mice was confirmed by an improved response to von Frey mechanical pain stimulation compared to 6-OHDA-injected WT littermates (Figure 5J). Chronic VEGF-D overexpression thus impacted dendritic rearrangements of adipose neurons with a compact somatic restructuring and high threshold to mechanical pain stimulation when challenged by an acute injury.

Adipose somatic reorganization remains unchanged across normal and obese Adipo-VD mice.

The neuroprotective effect of chronic VEGFR-3 signaling in Adipo-VD mice was next examined after 4-months of high fat diet feeding as a model of Type II diabetes and potential peripheral neuropathy [42]. Overall inflammation levels are similar to WT mice with no significant differences in TNFα or IL-6 having been reported in obeste Adipo-VD tissue by multiplex array measurement [18]. Adipo-VD (body weight: 52.3±0.4g) and WT (body weight: 53.1±0.3g) inguinal adipose tissue were volume imaged for MAP-2 sympathetic innervation (Figure 6A). The expanded adipose tissue gave an overall impression of reduced neural process density resulting from obese adipose tissue expansion. Quantitative morphometric analysis identified that obese Adipo-VD subcutaneous adipose neurons had significantly shorter dendrites (Figure 6B) with increased branching (Figure 6C) compared to obese WT mice. The average dendrite terminal filament length (Figure 6D) and filament volume were reduced in obese Adipo-VD adipose (Figure 6E) compared to the WT. The dendritic morphology and clustering were thus different in Adipo-VD tissue in a pattern similar to that identified in chow-fed conditions. Unlike in chow feeding, no difference in the subcutaneous adipose norepinephrine levels were measured in WT and Adipo-VD mice (Figure 6F). Serum norepinephrine levels were also equivalent (Figure 6G). No difference in L3-DRG ATF3 nuclear co-localization indicated an otherwise equivalent Adipo-VD sympathetic pathophysiology (Figure 6H, 6I). Interestingly, von Frey testing demonstrated a marginal improvement to mechanical pain sensitization in obese Adipo-VD mice after 4 months of elevated VEGF-D (Figure 6J). Thus, chronic VEGF-D overexpression in obese Adipo-VD may offer limited protection against obesity-induced tissue stress.

DISCUSSION

Under any physiological condition, dendritic and axonal branching, intersections and synaptic connections regulate neurotransmission [43]. Having been altered, this may play a role in peripheral neuropathies associated with aging, obesity, and diabetes [42, 44, 45]. While VEGFR-3 signaling has been predominantly associated with lymphangiogenesis, here we demonstrate that VEGFR-3 activity can serve as a potential neurotrophic signal regulating dendritic geometry in peripheral, adipose tissue neurons, similar to effects identified previously in central neurons [11]. Chronic overexpression of the murine VEGFR-3-specific ligand VEGF-D affords dendritic arborization changes mimicking neurosensitization in vivo. VEGFR-3 signaling also affords neuroprotection within the tissue in response to an acute 6-OHDA neurotoxic challenge. Developing and mature neurons derived from hiPSC-NSCs were also protected when chronically cultured with a VEGFR-3-specific ligand in vitro. Lymphangiogenic ligands may, therefore, also protect dendritic arborization during inflammatory stress (Figure 7).

Selective postnatal restructuring and degeneration of dendritic elements are essential for precise neural circuit establishment [46–49]. Regardless of the mechanism of dendritic reorganization [50, 51], a spontaneous or delayed restructuring and pruning of dendrites and axons is essential for stable neurite arbors [47, 50]. Dendritic and axonal arbor restructuring are further augmented by neurotrophic support, wherein essential neurons form robust

synaptic connections and secrete factors that eliminate weaker dendrites and axons [48, 52]. In vivo, VEGF-D-VEGFR-3 signaling has been shown to help prevent cell death and preserve dendritic structure during stroke-induced stress [10]. No patch clamp studies were performed in our study based on the recent findings that VEGF-D does not elicit sub-cellular voltage gradient and basal firing activity within neurons [53], but our data support a growing body of evidence that VEGF-D mediates dendritic complexity.

Vascular endothelial growth factors (VEGFs) and their receptors (VEGFRs) have been implied in the growth and remodeling of both the vasculature and sympathetic synaptic connections [12, 54]. These "vasculogenic" factors have been shown to drive adult neurogenesis and display neuroprotective and pro-survival properties in retinal ganglionic injury, stroke, and motor neuron injury models [10, 55, 56]. For example, signaling of VEGFR-2 [57], the most well-characterized angiogenic pathway, regulates neuronal branching and neuroprotection signaling via the canonical Akt and ERK signaling pathways [58]. While the "lymphangiogenic" factors, VEGF-C and VEGF-D, have been less well characterized in this context, convincing data demonstrate that VEGF-C and/or VEGFR-3 signaling drive enhanced neurogenesis in young NSCs and serve as a critical dendritic arborization maintenance factors in mouse hippocampal neurons [9, 11]. Our in vitro data demonstrates that developing and mature mVC-cultured neurons were resistant to 6-OHDA neurotoxicity. A similar chronic VEGFR-3 driven dendritic arborization pattern was mirrored in vivo when the tissue was challenged by acute 6-OHDA delivery to sympathetically denervate the adipose depot. VEGFR-3-specific signaling appears to impact dendrite arborization and branching, indicative of altered dendritic complexity. These changes were also seen in obese Adipo-VD tissue confirming that VEGF-D was the predominant driver and not the tissue's metabolic health. Neurons autoregulate BDNF isoform mediated synaptic clustering, cellular neuroprotection signaling pathways, dendritic dynamics and facilitate pruning of unwanted axons [40, 59, 60]. While we demonstrate that chronically treated developing mVC neurons significantly overexpress m-BDNF, our studies only suggest, but do not directly demonstrate, BDNF involvement in VEGFR-3-induced neuroprotection.

In humans, VEGF-C and VEGF-D predominantly signal on VEGFR-3 but also display some VEGFR-2 activity; murine VEGF-D is specific to VEGFR-3 [27]. This is important to consider when assessing past work. For example, in one study that determined VEGF-C to drive a dopaminergic phenotype in neurons, VEGFR-2 activation was identified as the pathway [34]. Another study, using human cells and human VEGF-D, identified dopaminergic differentiation attributed to VEGFR-3 signaling [33]. Our study found little difference in the neuronal phenotype of hiPSC-NSC derived neurons chronically cultured in the presence of the VEGFR-3-specific mVC protein: a change in the neuronal phenotype was therefore not a significant contributor to neuroprotection as. Importantly, tyrosine hydroxylase expressing cells are more susceptible to 6-OHDA stress, but these neurons were protected when cultured with mVC. The various potential signaling pathways of these ligands and receptors across species, however, may complicate the identification of VEGFR-3 protective cellular mechanisms.

There is also a growing appreciation for activity-dependent arbor restructuring and regeneration during inflammation and injury [61, 62]. Evidence suggests that adipose tissue pathophysiology during cold exposure affects arborization, activity, and neuroendocrine secretions [42]. The impact of adipose vascularization and sympathetic innervation on energy metabolism, lipolytic activity, and thermogenesis has received greater interest in the study of inflamed, obese adipose tissue [63]. VEGF-A, VEGF-B, and VEGF-D driven enhancements in adipose metabolic responsiveness have been previously reported in several publications and attributed to increased blood or lymphatic vascularization (well reviewed in: [64]). In Adipo-VD mice, for example, we have previously demonstrated that augmenting VEGF-D signaling and lymphangiogenesis in adipose tissue improves metabolic responsiveness during obesity [18]. Zhao and colleagues utilized a mouse model overexpressing VEGF-A in adipose tissue and identified increased sympathetic activity; the improved metabolic health in this mouse was previously attributed to tissue angiogenesis [65]. During adipose inflammation and obesity, sympathetic outflow also helps regulate the local inflammatory microenvironment [66–68]. Might changes in innervation and neuroendocrine secretions be potentially part of the increased metabolic responsiveness when activating VEGFRs?

The endogenous neurotransmitter norepinephrine locally controls antiinflammatory and inhibitory neurotransmission. We found that tissue norepinephrine levels inversely correlated with changes in the expression of the neuro-regeneration stress factor ATF-3 in the DRG in Adipo-VD mice (both with or without 6-OHDA, though the norepinephrine levels were opposite with stress), suggesting VEGFR-3 signaling potentially regulates afferent neuroprotective/inhibitory sympathetic output [69–72]. Changes in subcutaneous norepinephrine levels were identified in our chow fed Adipo-VD mice; whether this is a direct result of VEGFR-3 signaling was not demonstrated. While we did not see changes in norepinephrine levels in obese mice, the dendritic arborization and nociceptive sensitization response in Adipo-VD mice improved irrespective of the metabolic state. Coupled with findings in chow-fed animals and cultured neurons, this suggests that structural changes in dendrites coincide with metabolic and inflammatory outcomes of Adipo-VD mice.

In summary, we show that chronic VEGFR-3 signaling in vivo or in differentiating/ mature neurons induces a morphometric rearrangement of somatic dendrites and dendritic terminals. While this rearrangement mimics a post-injury response, VEGFR-3 upregulation preserves dendritic arborization and sympathetic outflow during stress. VEGFR-3 activation in neurons could therefore be neuroprotective and may play a role in neuropathic pain sensitization in chronic inflammatory disease.

Supplementary Material

Refer to Web version on PubMed Central for supplementary material.

Acknowledgements

REFERENCES

1. Pop-Busui R, et al. , Inflammation as a Therapeutic Target for Diabetic Neuropathies. Curr Diab Rep, 2016. 16(3): p. 29. [PubMed: 26897744]

2. Hozumi J, et al. , Relationship between Neuropathic Pain and Obesity. Pain Res Manag, 2016. 2016: p. 2487924. [PubMed: 27445603]

3. Tan AM, et al. , Maladaptive dendritic spine remodeling contributes to diabetic neuropathic pain. J Neurosci, 2012. 32(20): p. 6795–807. [PubMed: 22593049]

4. Flor H, Nikolajsen L, and Staehelin Jensen T, Phantom limb pain: a case of maladaptive CNS plasticity? Nat Rev Neurosci, 2006. 7(11): p. 873–81. [PubMed: 17053811]

5. Thompson-Peer KL, et al. , In vivo dendrite regeneration after injury is different from dendrite development. Genes Dev, 2016. 30(15): p. 1776–89. [PubMed: 27542831]

6. Luo C, Kuner T, and Kuner R, Synaptic plasticity in pathological pain. Trends Neurosci, 2014. 37(6): p. 343–55. [PubMed: 24833289]

7. Oliver G, et al. , The Lymphatic Vasculature in the 21(st) Century: Novel Functional Roles in Homeostasis and Disease. Cell, 2020. 182(2): p. 270–296. [PubMed: 32707093]

8. Abouelkheir GR, Upchurch BD, and Rutkowski JM, Lymphangiogenesis: fuel, smoke, or extinguisher of inflammation's fire? Exp Biol Med (Maywood), 2017. 242(8): p. 884–895. [PubMed: 28346012]

9. Han J, et al. , Vascular endothelial growth factor receptor 3 controls neural stem cell activation in mice and humans. Cell Rep, 2015. 10(7): p. 1158–72. [PubMed: 25704818]

10. Mauceri D, et al. , Nasally delivered VEGFD mimetics mitigate stroke-induced dendrite loss and brain damage. Proceedings of the National Academy of Sciences, 2020. 117(15): p. 8616.

11. Mauceri D, et al. , Nuclear calcium-VEGFD signaling controls maintenance of dendrite arborization necessary for memory formation. Neuron, 2011. 71(1): p. 117–30. [PubMed: 21745642]

12. Calvo C-F, et al. , Vascular endothelial growth factor receptor 3 directly regulates murine neurogenesis. Genes & development, 2011. 25(8): p. 831–844. [PubMed: 21498572]

13. Le Bras B, et al. , VEGF-C is a trophic factor for neural progenitors in the vertebrate embryonic brain. Nat Neurosci, 2006. 9(3): p. 340–8. [PubMed: 16462734]

14. Iglesias González PA, et al. , In vitro 6-hydroxydopamine-induced neurotoxicity: New insights on NFkB modulation. Toxicol In Vitro, 2019. 60: p. 400–411. [PubMed: 31247335]

15. Harris RBS, Sympathetic denervation of one white fat depot changes norepinephrine content and turnover in intact white and brown fat depots. Obesity (Silver Spring, Md.), 2012. 20(7): p. 1355–1364.

16. Zhu Y, et al. , Connexin 43 Mediates White Adipose Tissue Beiging by Facilitating the Propagation of Sympathetic Neuronal Signals. Cell metabolism, 2016. 24(3): p. 420–433. [PubMed: 27626200]

17. Lammoglia GM, et al. , Hyperplasia, de novo lymphangiogenesis, and lymphatic regression in mice with tissue-specific, inducible overexpression of murine VEGF-D. Am J Physiol Heart Circ Physiol, 2016. 311(2): p. H384–94. [PubMed: 27342876]

18. Chakraborty A, et al. , Vascular Endothelial Growth Factor-D (VEGF-D) Overexpression and Lymphatic Expansion in Murine Adipose Tissue Improves Metabolism in Obesity. The American Journal of Pathology, 2019. 189(4): p. 924–939. [PubMed: 30878136]

19. Chakraborty A, et al. , Characterizing Lymphangiogenesis and Concurrent Inflammation in Adipose Tissue in Response to VEGF-D. Frontiers in Physiology, 2020. 11(363).

20. Martinov T, et al. , Measuring changes in tactile sensitivity in the hind paw of mice using an electronic von Frey apparatus. J Vis Exp, 2013(82): p. e51212. [PubMed: 24378519]

21. Minett MS, Eijkelkamp N, and Wood JN, Significant Determinants of Mouse Pain Behaviour. PLOS ONE, 2014. 9(8): p. e104458. [PubMed: 25101983]

22. Emery MA, et al. , Burn injury decreases the antinociceptive effects of opioids. Behav Pharmacol, 2017. 28(4): p. 285–293. [PubMed: 28134661]

23. Sleigh JN, Weir GA, and Schiavo G, A simple, step-by-step dissection protocol for the rapid isolation of mouse dorsal root ganglia. BMC Res Notes, 2016. 9: p. 82. [PubMed: 26864470]

24. Jing D, et al. , Tissue clearing of both hard and soft tissue organs with the PEGASOS method. Cell Research, 2018. 28(8): p. 803–818. [PubMed: 29844583]

25. Yan Y, et al. , Efficient and rapid derivation of primitive neural stem cells and generation of brain subtype neurons from human pluripotent stem cells. Stem Cells Transl Med, 2013. 2(11): p. 862–70. [PubMed: 24113065]

26. Upadhya R, et al. , Extracellular vesicles from human iPSC-derived neural stem cells: miRNA and protein signatures, and anti-inflammatory and neurogenic properties. J Extracell Vesicles, 2020. 9(1): p. 1809064. [PubMed: 32944193]

27. Baldwin ME, et al. , Vascular endothelial growth factor D is dispensable for development of the lymphatic system. Mol Cell Biol, 2005. 25(6): p. 2441–9. [PubMed: 15743836]

28. Ying HS, Gottron FJ, and Choi DW, Assessment of cell viability in primary neuronal cultures. Curr Protoc Neurosci, 2001. Chapter 7: p. Unit7.18.

29. Vornov JJ, Tasker RC, and Coyle JT, Direct observation of the agonist-specific regional vulnerability to glutamate, NMDA, and kainate neurotoxicity in organotypic hippocampal cultures. Experimental Neurology, 1991. 114(1): p. 11–22. [PubMed: 1717307]

30. Meijering E, et al. , Design and validation of a tool for neurite tracing and analysis in fluorescence microscopy images. Cytometry A, 2004. 58(2): p. 167–76. [PubMed: 15057970]

31. Bird AD and Cuntz H, Dissecting Sholl Analysis into Its Functional Components. Cell Rep, 2019. 27(10): p. 3081–3096.e5. [PubMed: 31167149]

32. Fontes A, et al. , Generation of human-induced pluripotent stem cells (hiPSCs) using episomal vectors on defined Essential 8™ Medium conditions. Methods Mol Biol, 2013. 997: p. 57–72. [PubMed: 23546748]

33. Schwartz CM, et al. , Stromal factors SDF1a, sFRP1, and VEGFD induce dopaminergic neuron differentiation of human pluripotent stem cells. J Neurosci Res, 2012. 90(7): p. 1367–81. [PubMed: 22535492]

34. Piltonen M, et al. , Vascular endothelial growth factor C acts as a neurotrophic factor for dopamine neurons in vitro and in vivo. Neuroscience, 2011. 192: p. 550–63. [PubMed: 21767614]

35. Franchini L, et al. , Synaptic GluN2A-Containing NMDA Receptors: From Physiology to Pathological Synaptic Plasticity. International journal of molecular sciences, 2020. 21(4): p. 1538.

36. Yashiro K and Philpot BD, Regulation of NMDA receptor subunit expression and its implications for LTD, LTP, and metaplasticity. Neuropharmacology, 2008. 55(7): p. 1081–1094. [PubMed: 18755202]

37. Schlüter A, et al. , VEGFD Protects Retinal Ganglion Cells and, consequently, Capillaries against Excitotoxic Injury. Mol Ther Methods Clin Dev, 2020. 17: p. 281–299. [PubMed: 32055648]

38. Binley KE, et al. , Brain-derived neurotrophic factor prevents dendritic retraction of adult mouse retinal ganglion cells. Eur J Neurosci, 2016. 44(3): p. 2028–39. [PubMed: 27285957]

39. Ortiz JB, et al. , BDNF and TrkB Mediate the Improvement from Chronic Stress-induced Spatial Memory Deficits and CA3 Dendritic Retraction. Neuroscience, 2018. 388: p. 330–346. [PubMed: 30076998]

40. Orefice LL, et al. , Control of spine maturation and pruning through proBDNF synthesized and released in dendrites. Mol Cell Neurosci, 2016. 71: p. 66–79. [PubMed: 26705735]

41. Vaughan CH, et al. , Analysis and measurement of the sympathetic and sensory innervation of white and brown adipose tissue. Methods in enzymology, 2014. 537: p. 199–225. [PubMed: 24480348]

42. Blaszkiewicz M, et al. , Neuropathy and neural plasticity in the subcutaneous white adipose depot. PLoS One, 2019. 14(9): p. e0221766. [PubMed: 31509546]

43. Goaillard J-M, et al. , Diversity of Axonal and Dendritic Contributions to Neuronal Output. Frontiers in Cellular Neuroscience, 2020. 13(570).

44. Cheng C, et al. , Loss of innervation and axon plasticity accompanies impaired diabetic wound healing. PLoS One, 2013. 8(9): p. e75877. [PubMed: 24098736]

45. Stratton HJ and Khanna R, Sculpting Dendritic Spines during Initiation and Maintenance of Neuropathic Pain. J Neurosci, 2020. 40(40): p. 7578–7589. [PubMed: 32998955]

46. Sakai J, Core Concept: How synaptic pruning shapes neural wiring during development and, possibly, in disease. Proc Natl Acad Sci U S A, 2020. 117(28): p. 16096–16099. [PubMed: 32581125]

47. Stephan AH, Barres BA, and Stevens B, The complement system: an unexpected role in synaptic pruning during development and disease. Annu Rev Neurosci, 2012. 35: p. 369–89. [PubMed: 22715882]

48. Riccomagno MM and Kolodkin AL, Sculpting neural circuits by axon and dendrite pruning. Annu Rev Cell Dev Biol, 2015. 31: p. 779–805. [PubMed: 26436703]

49. Lin Y-C and Koleske AJ, Mechanisms of synapse and dendrite maintenance and their disruption in psychiatric and neurodegenerative disorders. Annual review of neuroscience, 2010. 33: p. 349–378.

50. Riccomagno MM and Kolodkin AL, Sculpting Neural Circuits by Axon and Dendrite Pruning. Annual Review of Cell and Developmental Biology, 2015. 31(1): p. 779–805.

51. Sainath R and Gallo G, Cytoskeletal and signaling mechanisms of neurite formation. Cell and tissue research, 2015. 359(1): p. 267–278. [PubMed: 25080065]

52. Bagri A, et al. , Stereotyped pruning of long hippocampal axon branches triggered by retraction inducers of the semaphorin family. Cell, 2003. 113(3): p. 285–99. [PubMed: 12732138]

53. Maurer J, et al. , VEGF-D Downregulation in CA1 Pyramidal Neurons Exerts Asymmetric Changes of Dendritic Morphology without Correlated Electrophysiological Alterations. Neuroscience, 2020. 448: p. 28–42. [PubMed: 32920043]

54. Rosenstein JM, Krum JM, and Ruhrberg C, VEGF in the nervous system. Organogenesis, 2010. 6(2): p. 107–114. [PubMed: 20885857]

55. Poesen K, et al. , Novel role for vascular endothelial growth factor (VEGF) receptor-1 and its ligand VEGF-B in motor neuron degeneration. The Journal of neuroscience : the official journal of the Society for Neuroscience, 2008. 28(42): p. 10451–10459. [PubMed: 18923022]

56. Froger N, et al. , VEGF is an autocrine/paracrine neuroprotective factor for injured retinal ganglion neurons. Scientific Reports, 2020. 10(1): p. 12409. [PubMed: 32710087]

57. Harde E, et al. , EphrinB2 regulates VEGFR2 during dendritogenesis and hippocampal circuitry development. Elife, 2019. 8.

58. Hao T and Rockwell P, Signaling through the vascular endothelial growth factor receptor VEGFR-2 protects hippocampal neurons from mitochondrial dysfunction and oxidative stress. Free radical biology & medicine, 2013. 63: p. 421–431. [PubMed: 23732519]

59. Hu B, Nikolakopoulou AM, and Cohen-Cory S, BDNF stabilizes synapses and maintains the structural complexity of optic axons in vivo. Development, 2005. 132(19): p. 4285–98. [PubMed: 16141221]

60. Niculescu D, et al. , A BDNF-Mediated Push-Pull Plasticity Mechanism for Synaptic Clustering. Cell Rep, 2018. 24(8): p. 2063–2074. [PubMed: 30134168]

61. Udina E, et al. , Effects of activity-dependent strategies on regeneration and plasticity after peripheral nerve injuries. Ann Anat, 2011. 193(4): p. 347–53. [PubMed: 21514121]

62. Fauth M and Tetzlaff C, Opposing Effects of Neuronal Activity on Structural Plasticity. Frontiers in Neuroanatomy, 2016. 10(75).

63. Bartness TJ, et al. , Sensory and sympathetic nervous system control of white adipose tissue lipolysis. Mol Cell Endocrinol, 2010. 318(1-2): p. 34–43. [PubMed: 19747957]

64. Fang Y, Kaszuba T, and Imoukhuede PI, Systems Biology Will Direct Vascular-Targeted Therapy for Obesity. Front Physiol, 2020. 11: p. 831. [PubMed: 32760294]

65. Zhao Y, et al. , Transient Overexpression of Vascular Endothelial Growth Factor A in Adipose Tissue Promotes Energy Expenditure via Activation of the Sympathetic Nervous System. Mol Cell Biol, 2018. 38(22).

66. Wang Y.-h., et al. , Adipose Stem Cell-Based Clinical Strategy for Neural Regeneration: A Review of Current Opinion. Stem Cells International, 2019. 2019: p. 8502370. [PubMed: 31827536]

67. Tang L, et al. , Sympathetic Nerve Activity Maintains an Anti-Inflammatory State in Adipose Tissue in Male Mice by Inhibiting TNF-α Gene Expression in Macrophages. Endocrinology, 2015. 156(10): p. 3680–94. [PubMed: 26132918]

68. Udit S, et al. , Na(v)1.8 neurons are involved in limiting acute phase responses to dietary fat. Mol Metab, 2017. 6(10): p. 1081–1091. [PubMed: 29031710]

69. Seijffers R, Mills CD, and Woolf CJ, ATF3 increases the intrinsic growth state of DRG neurons to enhance peripheral nerve regeneration. J Neurosci, 2007. 27(30): p. 7911–20. [PubMed: 17652582]

70. Gautron L, Toward a Neuroimmunoendocrinology of Adipose Tissue. Endocrinology, 2015. 156(10): p. 3485–3487. [PubMed: 26380935]

71. Tsujino H., et al. , Activating transcription factor 3 (ATF3) induction by axotomy in sensory and motoneurons: A novel neuronal marker of nerve injury. Mol Cell Neurosci, 2000. 15(2): p. 170–82. [PubMed: 10673325]

72. Bloechlinger S, Karchewski LA, and Woolf CJ, Dynamic changes in glypican-1 expression in dorsal root ganglion neurons after peripheral and central axonal injury. Eur J Neurosci, 2004. 19(5): p. 1119–32. [PubMed: 15016071]

HIGHLIGHTS

- Chronic "lymphangiogenic" VEGFR-3 signaling induces dendritic structure remodeling in vivo.

- VEGFR-3 reduces dendritic length and terminal filament length/volume with increased branching.

- VEGFR-3 driven dendritic arborization changes are also demonstrated in hiPSC-NSC derived neurons.

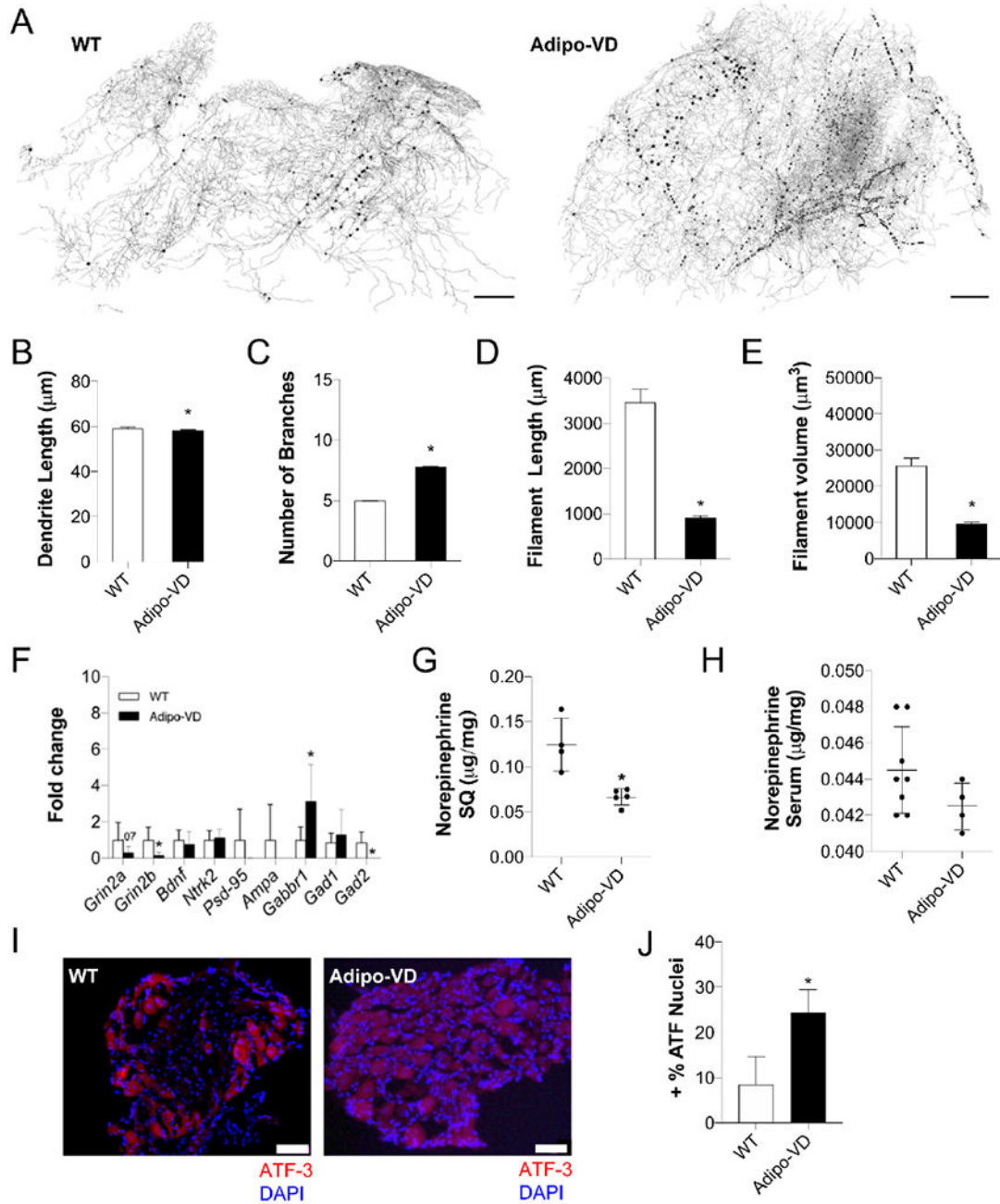- VEGFR-3 activated neurons demonstrate protection from 6-OHDA stress in vitro and in vivo.

Figure 1. Chronically elevated VEGF-D levels impact subcutaneous adipose tissue innervation.
(A) Volume imaging of subcutaneous adipose neuronal structures in wild type: WT
(−rtTA) and Adipo-VD (+rtTA) chow mice; (Map-2, set as grey scale for visual clarity).
(B) Comparison of adipose dendrite length (measured from the cell body); (C) dendrite
branching; (D) dendritic terminal filament length; and (E) dendritic terminal filament
volume in adipose between WT and Adipo-VD mice. (F) RT-qPCR of neuronal phenotype
genes in 1-month Adipo-VD mice normalized to ubiquitin and compared to WT tissue.
(G) Norepinephrine within WT and Adipo-VD inguinal adipose per mg protein. (H) Serum

norepinephrine levels in WT and Adipo-VD mice. (I) ATF3+ (red) positive nuclei (blue) in L3 dorsal root ganglia (DRG) of WT and Adipo-VD mice. (J) Comparison of the ratio of ATF3+ positive nuclei vs total DRG cell body nuclei of WT and Adipo-VD mice. (A) n=3,3; scale bar= 200 μm (B-E) n=3,3 (F) n=6,6 (G) n=4,5 (H) n=8,4 (I-J) n=4,4. *p<0.05 vs −rtTA (B-E) mean ± SEM (F, G, H, J) mean ± SD.
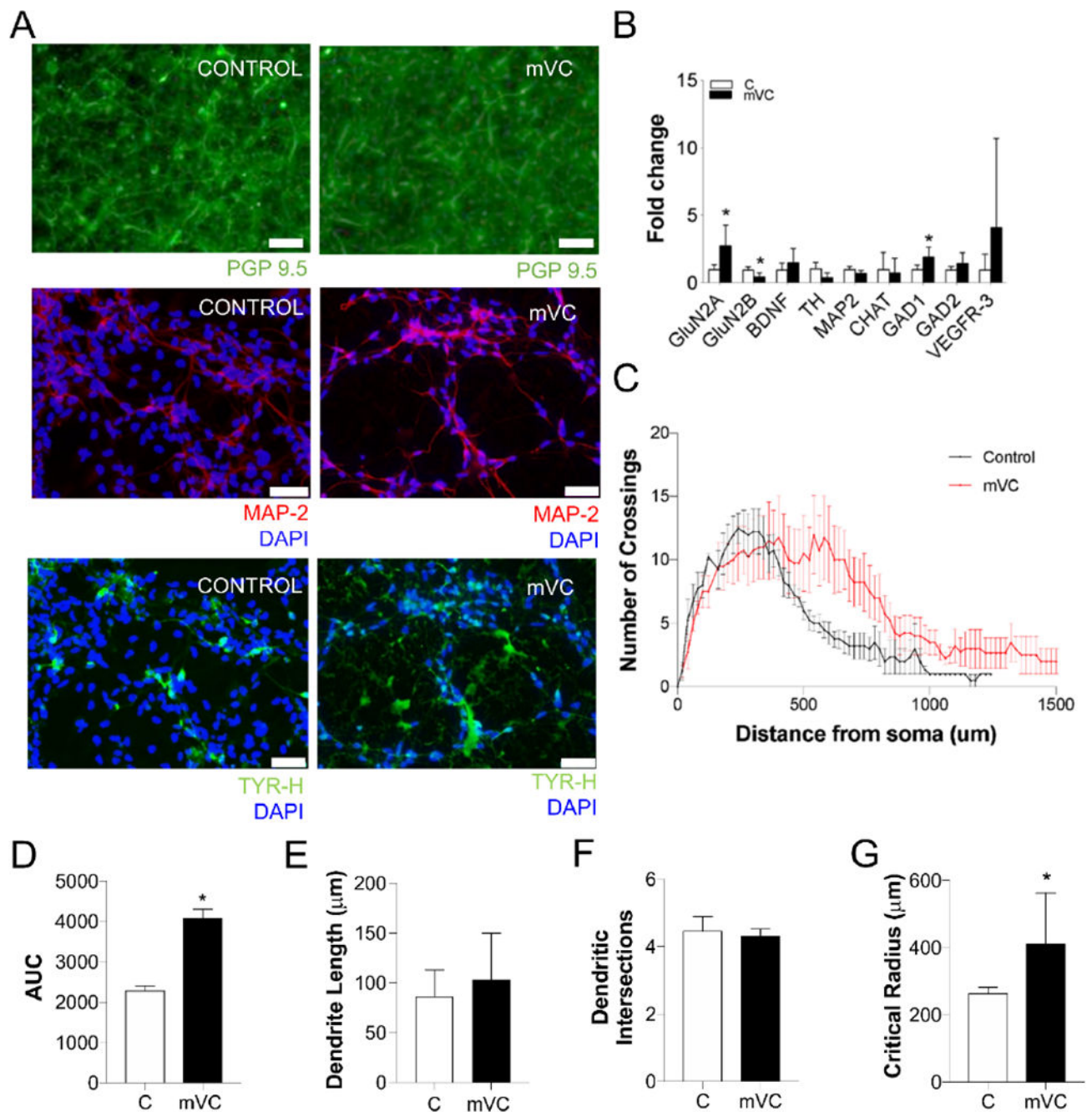
Figure 2. Developing neurons differentiated in the presence of VEGFR-3 ligand results in minimal phenotypic change

(A) hiPSC-NSC control and mVC (VEGFR-3-specific mutant VEGF-C) neurons phenotypically characterized using PGP9.5 (green), MAP-2 (red), tyrosine-hydroxylase-TYR-H (green) and DAPI (blue). (B) RT-qPCR of neuronal phenotype genes and *VEGFR-3* gene expression were compared between control and mVC neurons at day 31. (C) Sholl quantification of total dendritic intersections of hiPSC-NSC control and mVC neurons. (D) Area under the curve (AUC); (E) dendrite length; (F) dendrite intersection; and (G) critical radius of the dendrite processes calculated from Sholl intersections. (A) PGP 9.5 scale bar=

100 μm. MAP-2and TH scale bar= 20 μm n=2, (B) n=10 Bars represent mean ± SD (C-G) n=10,10 Statistically significant differences are indicated with asterisks, *p < 0.005. Bars represent mean ± SEM.
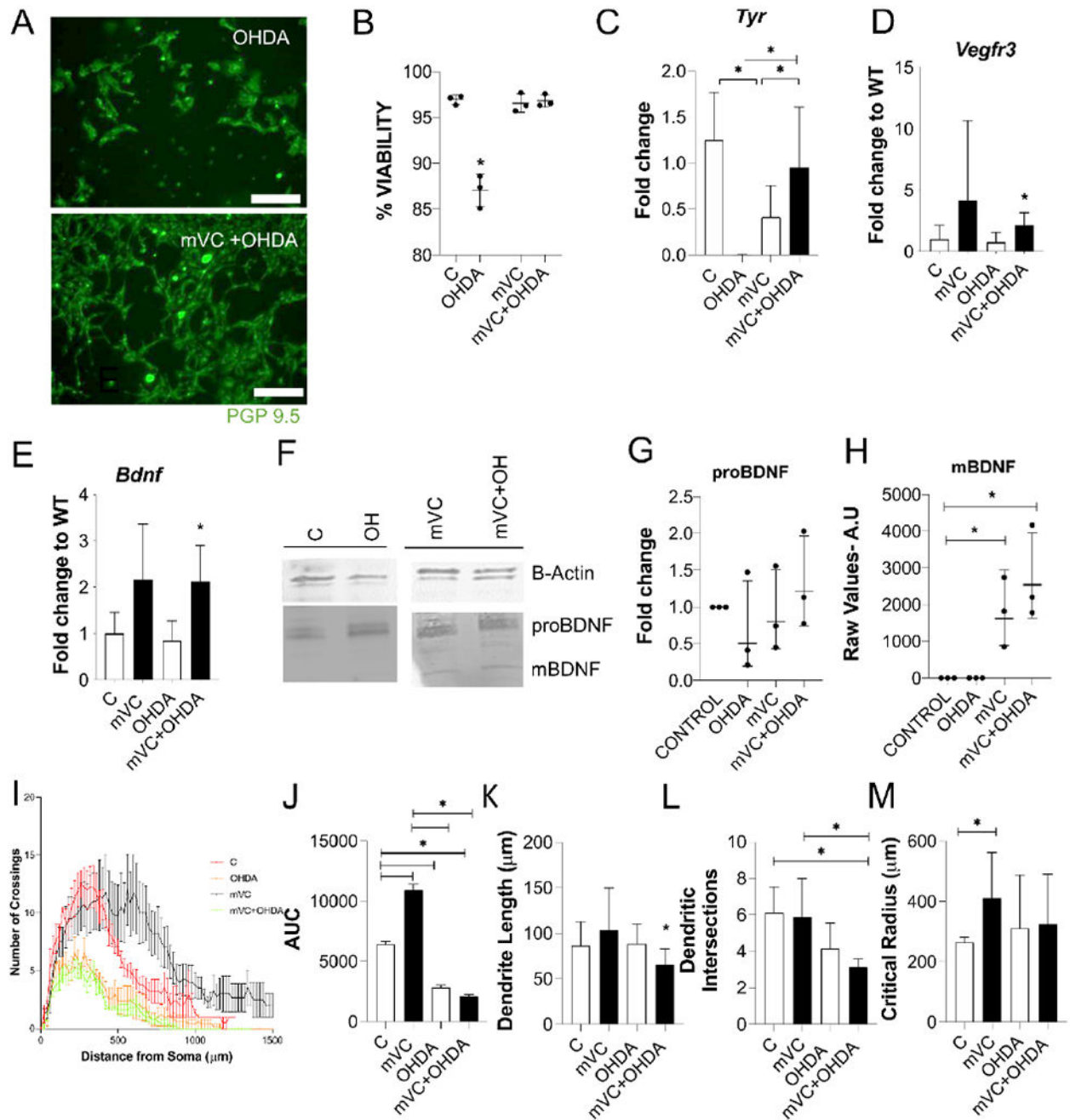
Figure 3. Developing neurons differentiated in the presence of chronic VEGFR-3 ligand display improved dendritic arbor restructuring in-vitro

(A) hiPSC- Neural Stem Cell (NSC) control and mVC (VEGFR-3-specific mutant VEGF-C) neurons after 2 hrs. of 6-hydroxydopamine (6-OHDA represented as OHDA in figures) treatment PGP9.5 (green). (B) PI/trypan Blue exclusion assay based % viable cells calculated across various treatments. (C) RT-qPCR fold change of *TYR* expression between control, mVC, 6-OHDA and mVC-6-OHDA treated neurons. (D) RT-qPCR of *VEGFR-3* gene expression compared between control, mVC, 6-OHDA and mVC-6-OHDA day 31 neurons. (E) RT-qPCR of *BDNF* gene expression. (F) BNDF immunoblot. (G) pro-BDNF

represented as fold change and (H) mature-BDNF represented as raw densitometric arbitrary unit values across neurons with various treatments groups. (I) Quantification of total dendritic intersections through Shall analysis of hiPSC-NSC control, mVC, 6-OHDA and mVC-6-OHDA neurons. (J) Area under the curve (AUC); (K) dendrite length; (L) dendrite intersections; and (M) critical radius of the dendrite processes. (A) PGP 9.5 scale bar= 100 μm, n=2, (B-E) n=10,10 (F, G, H) n=3, (I, J, K, L, M) n=10. Statistically significant differences are indicated with asterisks, *p < 0.005, (B, C, D, E, G, H) Bars represent mean ± SD, (J, K, L, M) Bars represent mean ± SEM.
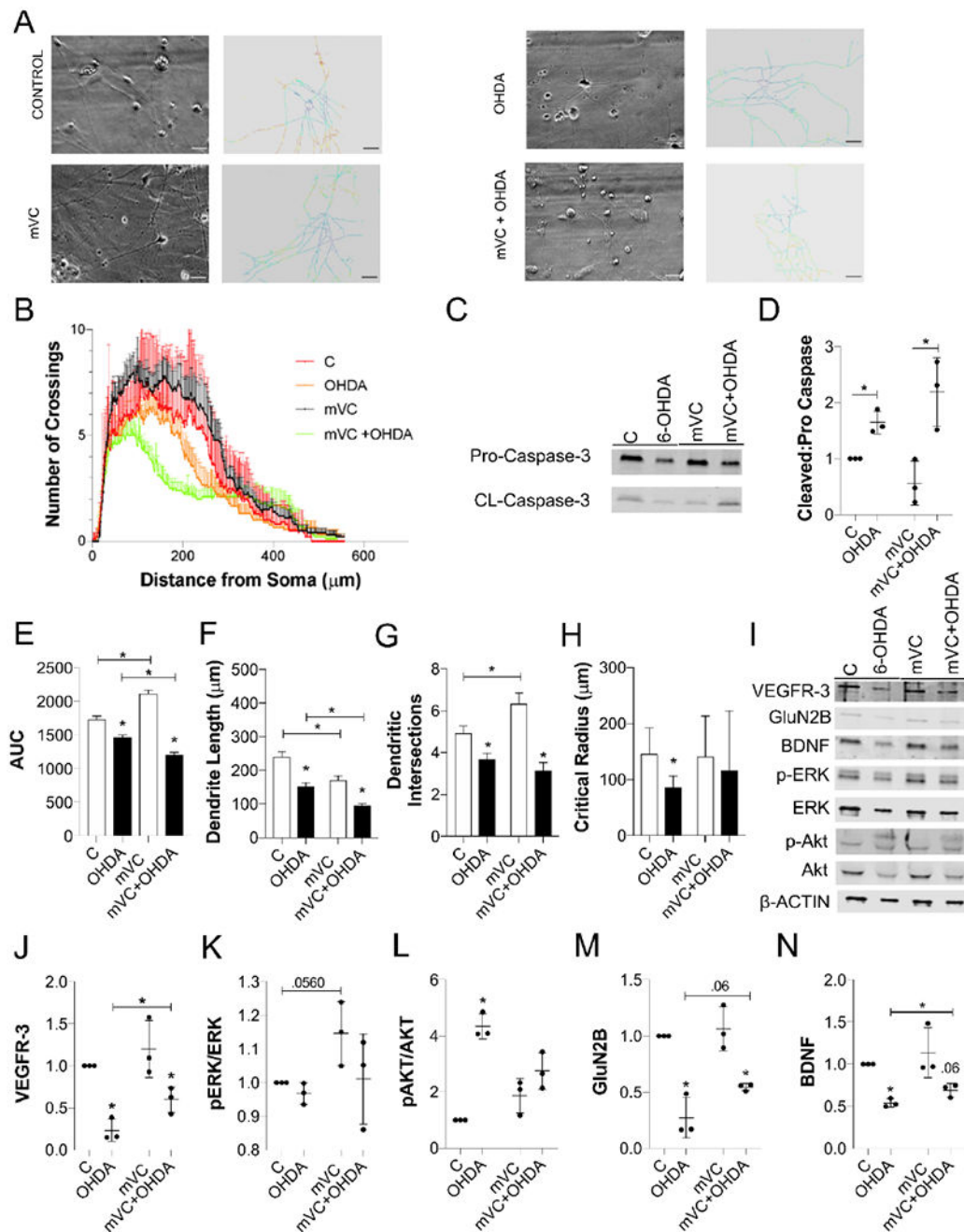
Figure 4. Effects of acute VEGFR-3 activation in hiPSC-Neural Stem Cell (NSC) derived neurons

(A) Representative raw and skeletonized Sholl intersection micrograph of hiPSC-NSC (control, VEGFR-3-specific mutant VEGF-C (mVC), 6-hydroxydopamine (6-OHDA represented as OHDA in figures) and mVC+6-OHDA) neurons. (B) Quantification of total dendritic length, intersections through Sholl analysis. (C, D) Immunoblot and quantified ratio of cleaved:pro caspase across the treatment conditions. (E) Area under the curve (AUC); (F) dendrite length; (G) dendritic intersections; (H) and critical radius of the dendrite processes calculated from Sholl intersections. (I) Immunoblot analysis by using

phosphospecific antibodies of hiPSC-NSC neurons with or without mVC and 6-OHDA treatment. (J) Quantification of the immunoblot for VEGFR-3; (K) pERK/Total ERK; (L) pAKT/Total AKT; (M) GluN2B; and (N) BDNF (A) Original scale bar= 100 μm, images cropped with scales adjusted to 100 μm, n=10 (B,E,F,G,H) n=10 (C,D,I-N) n=3 Statistically significant differences are indicated with asterisks, *p < 0.005, (E-H) Bars represent mean ± SEM. (D,J-N) Bars represent mean ± SD.
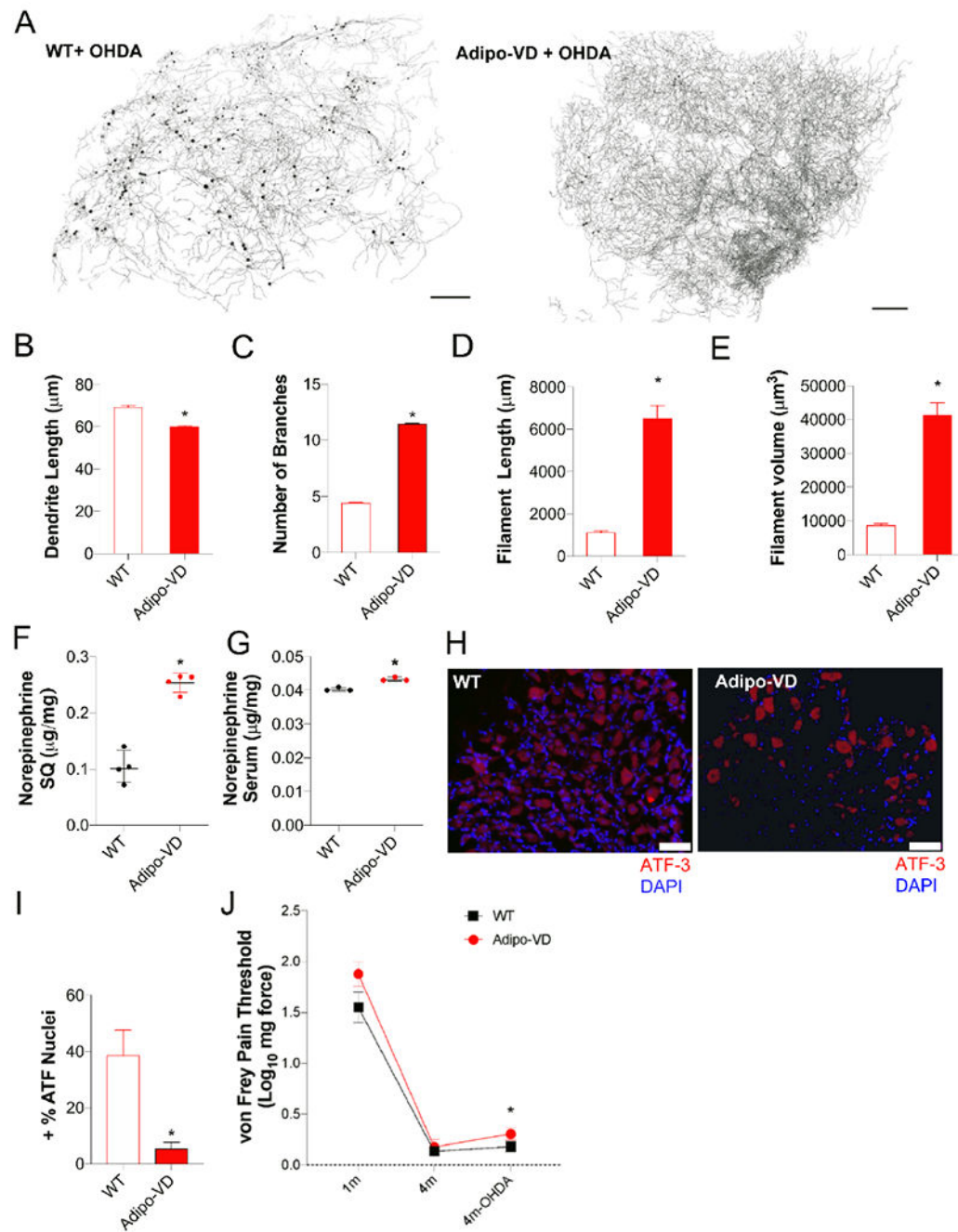
Figure 5. Chronically elevated VEGF-D levels protect inguinal adipose tissue innervation against injury.

(A) Volume imaging of subcutaneous adipose neuronal structures in wild type: WT (−rtTA) and Adipo-VD (+rtTA) chow mice after the injection of 6-hydroxydopamine (represented as OHDA in the figure) in the tissue; (Map-2, set as grey scale for visual clarity).

(B) Comparison of adipose dendrite length (measured from the cell body); (C) dendrite branching; (D) dendritic terminal filament length; and (E) dendritic terminal filament volume in adipose between WT and Adipo-VD mice after OHDA. (F) Norepinephrine level within WT and Adipo-VD inguinal adipose per mg protein. (G) Serum Norepinephrine

levels of WT and Adipo-VD mice. (H) ATF3+ (red) positive nuclei (blue) in L3 dorsal root ganglia (DRG) of WT and Adipo-VD mice. (I) Comparison of the ratio of ATF3+ positive nuclei vs total DRG cell body nuclei of WT and Adipo-VD mice. (J) Von-Frey pain threshold fold change comparison between WT and Adipo-VD quantified following 1 and 4-month chow diet feeding (+/− 6-OHDA) and all values normalized to WT reading at 1 month. (A) n=3,3 Grey Scale=MAP-2, scale bar= 200 μm (B-E) n=3,3 (F) n=4,4 (G) n=3,3 (H-I) n=4,4 (J) n=40. *p<0.05 vs WT (B-E) mean ± SEM (F, G, I, J) mean ± SD.
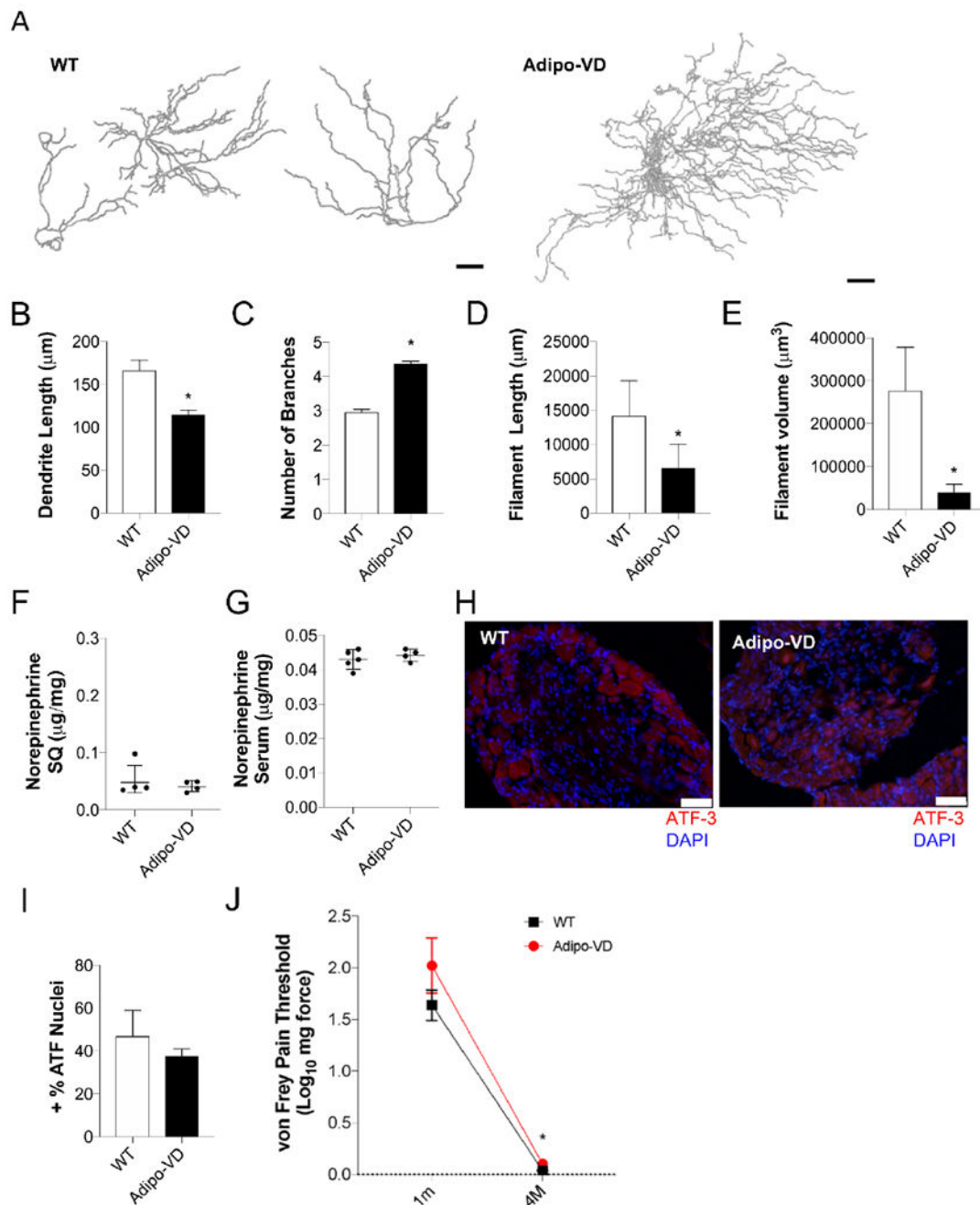
Figure 6. Tissue innervation in Adipo-VD obese remains unchanged across normal and obese Adipo-VD mice.

(A) Volume imaging of subcutaneous adipose neuronal structures in wild type: WT (−rtTA) and Adipo-VD (+rtTA) high fed diet (HFD) mice; (Map-2, set as grey scale for visual clarity). (B) Comparison of adipose dendrite length (measured from the cell body); (C) dendrite branching; (D) dendritic terminal filament length; and (E) dendritic terminal filament volume in adipose between obese WT and Adipo-VD mice. (F) Norepinephrine concentration within obese WT and Adipo-VD inguinal adipose per mg protein. (G) Serum Norepinephrine levels in obese WT and Adipo-VD mice. (H) ATF3+ (red) positive nuclei

(blue) in L3 dorsal root ganglia (DRG) of obese WT and Adipo-VD mice. (I) Comparison of the ratio of ATF3+ positive nuclei vs total DRG cell body nuclei of WT and Adipo-VD mice. (J) Von-Frey pain threshold fold change comparison between WT and Adipo-VD quantified following 1 and 4-month HFD diet feeding and all values normalized to WT reading at 1 month. (A) n=3,3 Grey Scale=MAP-2, scale bar= 200 μm (B-E) n=3,3 (F) n=4,4 (G) n=5,4 (H, I) n=4,4 (J) n=36. *p<0.05 vs WT (B-E) mean ± SEM (F, G, I, J) mean ± SD.
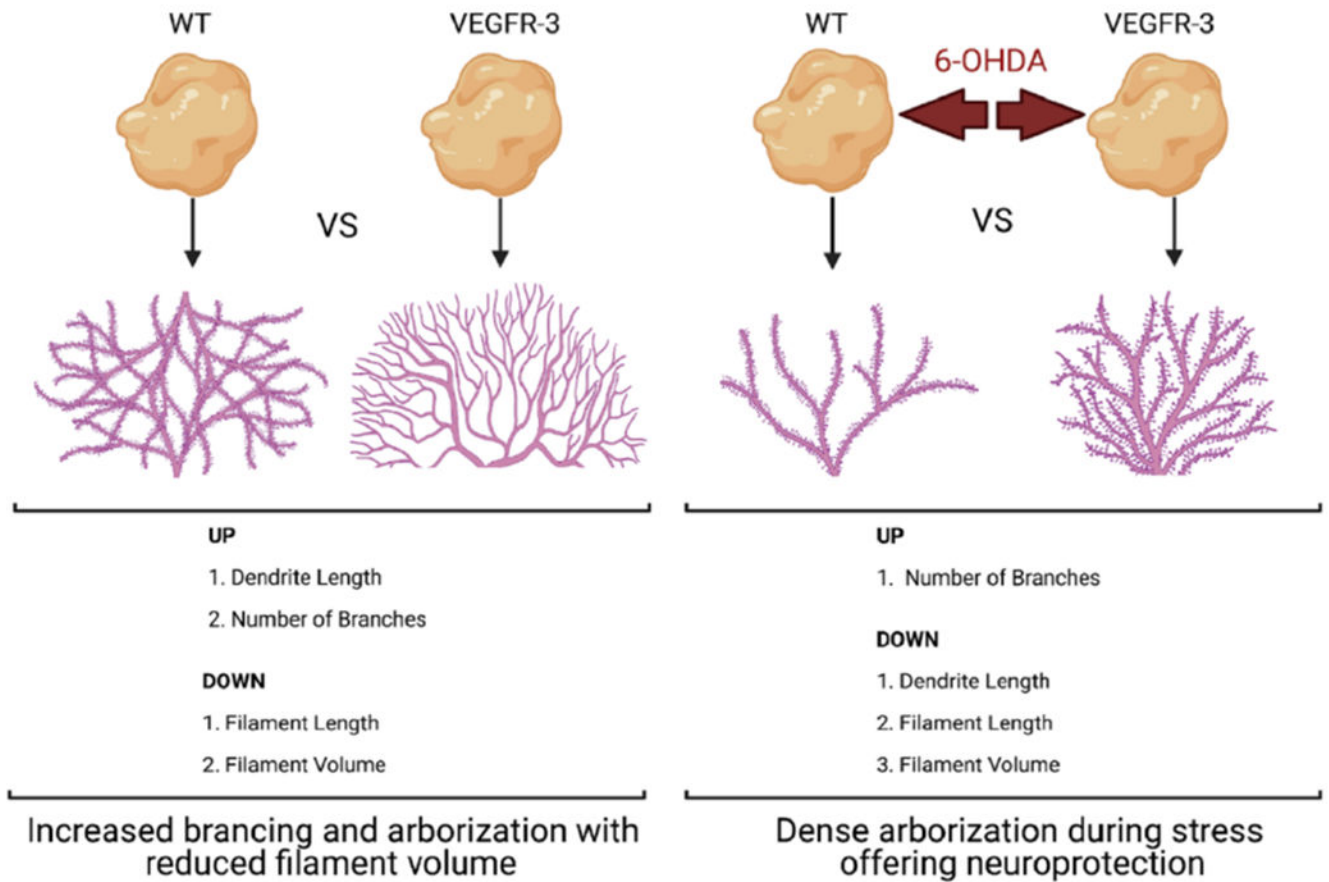
Figure 7. Figure summarizing neuronal innervation changes in Adipo-VD mice.
Chronic over expression of the VEGFR-3 ligand VEGF-D in the tissue of Adipo-VD mice alters neuronal dendrite morphology, length, branching, dendritic terminal filament volume and dendritic terminal filament length. This dense arborization response is protective against 6-hydroxydopamine (6-OHDA) neurotoxic stress in vivo and also in cultured neurons. Created with Biorender.com.

Table 1.

Primary antibodies utilized in this study.

Antigen	Source	Catalog number	RRID
AKT	Cell Signaling	4685	AB_2225340
pAKT	Cell Signaling	4060	AB_2315049
β-Actin	Sigma	A2228	AB_476697
BDNF	Thermo Fisher Scientific	OSB00017W	AB_10709559
CASPASE-3	Cell Signaling	9662S	AB_331439
GluN2B	Abcam	AB65783	AB_1658870
MAP2	Millipore	AB5622	AB_91939
VEGFR-3	R&D Systems	AF743	AB_355563
ERK	Cell Signaling	4696	AB_390780
pERK	Cell Signaling	4377S	AB_331775

Table 2.

Primer sequences utilized for qPCR in this study.

Gene-Human	Forward	Reverse
BDNF	GGCTTGACATCATTGGCTGAC	CATTGGGCCGAACTTTCTGGT
CHAT	GACCAGCTAAGGTTTGCAGC	CAGGAAGCCGGTATGATGAGA
GAD1	GCGGACCCCAATACCACTAAC	CACAAGGCGACTCTTCTCTTC
GAD2	TTTTGGTCTTTCGGGTCGGAA	TTCTCGGCGTCTCCGTAGAG
GLUN2B	TCTGACCGGAAGATCCAGGG	TCCATGATGTTGAGCATTACGG
GLUN2A	GACCCCAAGAGCCTCATCAC	CTGGATGGACGCTCCAAACT
MAP2	CTCAGCACCGCTAACAGAGG	CATTGGCGCTTCGGACAAG
NRP1	GACAAATGTGGCGGGACCATA	TGGATTAGCCATTCACACTTCTC
NRP2	GCTGGCTATATCACCTCTCCC	TCTCGATTTCAAAGTGAGGGTTG
TYR-H	GGAAGGCCGTGCTAAACCT	GGATTTTGGCTTCAAACGTCTC
VEGFR-3	TGCACGAGGTACATGCCAAC	GCTGCTCAAAGTCTCTCACGAA
Gene-Mouse	**Forward**	**Reverse**
Ampar	AGACCACCGAGGTCAAGATG	CGTCACCAAGTTGATCTCTGG
Bdnf	TCATACTTCGGTTGCATGAAGG	AGACCTCTCGAACCTGCCC
Gabbr1	AAAAGTCGGGGTCTCTCTGAC	CAGTCGGTCCAAAATTCTTGTGA
Gad1	CACAGGTCACCCTCGATTTTT	ACCATCCAACGATCTCTCTCATC
Gad2	TCCGGCTTTTGGTCCTTCG	ATGCCGCCCGTGAACTTTT
Grin2a	ACGTGACAGAACGCGAACTT	TCAGTGCGGTTCATCAATAACG
Grin2b	GCCATGAACGAGACTGAC	GCTTCCTGGTCCGTGTCA
Ntrk2	CTGGGGCTTATGCCTGCTG	AGGCTCAGTACACCAATCCTA
Psd-95	TGGATCCTGTGTCCCTCATA	GGGAGGAGACAAAGTGGTAATC